IOP Conf. Series: Journal of Physics: Conf. Series **1037** (2018) 022042 doi:10.1088/1742-6596/1037/2/022042

Probabilistic Design of Airfoils for Horizontal Axis Wind Turbines

R. Pereira, G. de Oliveira, W. A. Timmer and E. Quaeghebeur
Kluyverweg 1, 2629 HS Delft, NL
E-mail: r.b.santospereira@tudelft.nl

Abstract. We describe a probabilistic approach to design airfoils for wind energy applications. An analytical expression is derived for the probability of perturbations to the operational blade-section angle of attack. It includes the combined influence of wind shear, yaw-misalignment, and turbulence intensity. The theoretical fluctuations in angle of attack are validated against an aero-structural simulation of a 10 MW horizontal axis wind turbine, operating under different inflow conditions. Finally we incorporate the probabilistic approach into a multi-objective airfoil optimization problem, which is solved with a genetic algorithm. The results illustrate the compromise between airfoil performance for a specific angle of attack and robustness of airfoil performance over a large range of angle of attack fluctuations.

1. Introduction

When designing airfoils for horizontal axis wind turbine blades, different arguments are typically considered. Towards the blade tip aerodynamic performance is of paramount importance, leading to thin airfoil sections, while for inboard stations structural requirements result in stiff—and hence thick—profiles. Within desirable aerodynamic characteristics, different requirements are often aimed for. A large design lift contributes to aerodynamic damping [1] and may lead to a reduced chord, whereas a large lift-to-drag ratio allows for increased power extraction for a given rotor area. Additionally, roughness insensitivity is fundamental in wind energy airfoils [2, 3] mostly because leading edge soiling is often present and leads to early boundary layer transition.

Next to all these requirements, horizontal axis wind turbine blade sections continuously experience oscillations in the angle of attack (AOA), mostly due to the non-uniform wind velocity field and structural vibrations [4]. As such, and besides the several aerodynamic requirements for wind energy airfoils mentioned above,a point design [5] type of airfoil is not adequate. To tackle this issue, we introduce a probabilistic approach to take AOA fluctuations into account when designing airfoils. Three different sources of AOA perturbation are addressed (section 2): the influence of wind shear, yaw misalignment, and turbulence.

For the airfoil design itself, we define a multi-objective optimization problem, solved with a genetic algorithm [6, 7]. The cost function definition and the optimization set-up are described in section 4.

2. Probability of AOA fluctuations for specific blade sections

In this section we employ an analytical approach to describe three different sources of perturbations in angle of attack. Rotor yaw misalignment and wind shear are treated with a deterministic

method, whereas the influence of atmospheric turbulence is included using a probabilistic method. Finally, the combined probability of the different sources of AOA fluctuations is addressed.

2.1. Yaw misalignment

The convention of the reference frame used to describe the geometry of the problem is defined in Figures 1a and 1c, where the rotor-fixed orthogonal reference frame XYZ, yaw misalignment angle β and azimuthal angle ψ are shown.

For simplicity, we assume that the rotor does not have a prebend or cone angle, and that the blades are infinitely stiff. In practice this means that all blade sections are rotating in the same plane. We also assume that the undisturbed, free-stream wind velocity $\vec{U}$ does not have a vertical component while its magnitude U depends on the vertical coordinate, i.e. on height (cf. figure 1b). So $\vec{U} = U_X\vec{1}_X + U_Y\vec{1}_Y$ with

$$U_X = U\cos\beta \qquad \text{and} \qquad U_Y = -U\sin\beta \tag{1}$$

following the convention of figure 1c. The geometric effect of yaw misalignment on U_X and U_Y seen above is called the *advancing and retreating blade effect* [8].

Under these assumptions it is possible to define the wind speed U_r at the rotor for the radial position r along the blade. This is done by including the yaw misalignment effect and using the azimuth angle to parametrize the wind speed variation:

$$U_{rX} = U_X(1 - \bar{a} - K\sin\psi) \qquad \text{and} \qquad U_{rY} = U_Y. \tag{2}$$

The axial X-component U_{rX} of the wind speed at the rotor plane includes the azimuthally varying induction felt at the rotor—also termed *skewed wake effect*—modelled according to Pitt

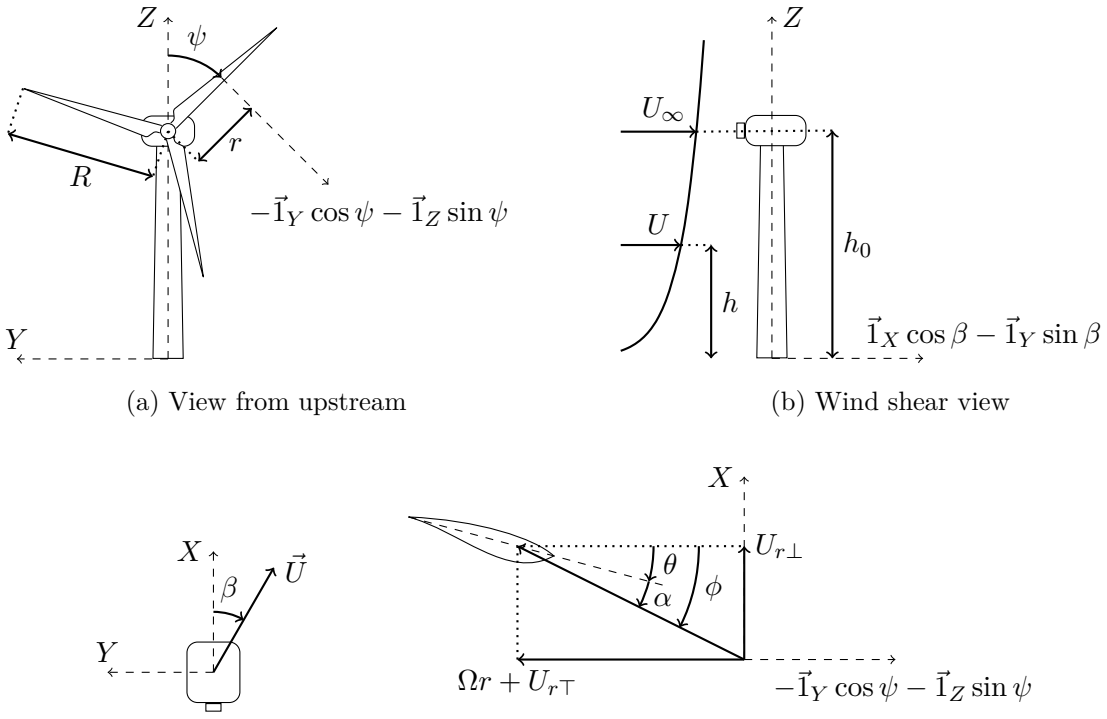

(a) View from upstream

(b) Wind shear view

(c) View from above

(d) View of blade section

Figure 1: Convention for the reference frame, angles, and notation

and Peters [9]. The symbol $\bar{a}$ denotes the azimuthally and radially averaged axial induction factor and K is a parameter which depends on the radial coordinate and yaw misalignment according to

$$K = \frac{15\pi}{32}\frac{r}{R}\tan\left(\frac{\beta(0.6\bar{a}+1)}{2}\right), \tag{3}$$

where R is the rotor radius. Expression 2 also shows that we assume the Y-component of the rotor induction is negligible, which is correct if the yaw misalignment is not large.

Since we wish to estimate the fluctuations of the angle of attack, it is necessary to express the wind speed components in the reference frame of the blade section. Recalling the assumption that all blade sections rotate in the same plane and relating Figures 1a and 1d, we can write

$$U_{r\perp} = U_{rX} \qquad \text{and} \qquad U_{r\top} = U_{rY}\cos\psi, \tag{4}$$

in which the subscripts $\perp$ and $\top$ denote the direction normal and tangential to the plane of rotation respectively.

2.2. Wind shear

We also model the effect of wind shear on the blade section AOA fluctuations. Notice that the blade section height h is determined by the radial coordinate r and the azimuth angle ψ. Specifically, folltitleowing the convention from figure 1b, it holds that $h = h_0 + r\cos\psi$, where h_0 represents the HAWT hub height. The logarithmic wind shear law [10] then gives

$$U = U_\infty \frac{\ln h - \ln z_0}{\ln h_0 - \ln z_0} = U_\infty \frac{\ln\left(h_0 + r\cos\psi\right) - \ln z_0}{\ln h_0 - \ln z_0}, \tag{5}$$

where U_∞ represents the undisturbed wind speed magnitude at hub height and z_0 is the roughness length.

2.3. Atmospheric turbulence

Similarly to what is presented in [7], the influence of atmospheric turbulence is introduced by considering a relative perturbation δ to the wind speed dependent on the turbulence intensity [11]. We here consider only turbulence induced wind speed perturbations in the X direction. This is justified both because the longitudinal (aligned with X) turbulence intensity is larger than the lateral (aligned with Y) component [12] and because the impact of longitudinal turbulence on AOA fluctuations is much larger than for other directions due to the relative velocity components at the blade section level (also illustrated in figure 1d).

Let $\vec{V}$ be the *turbulent* wind velocity, thefore its normal and tangential components are

$$V_{r\perp} = U_{r\perp}(1+\delta) \qquad \text{and} \qquad V_{r\top} = U_{r\top}, \tag{6}$$

so with $U_{r\perp}\delta$ as the instantaneous fluctuation.

2.4. Combination of perturbation sources

Having identified the individual contribution of each perturbation source, it is finally possible to combine equations 1 to 6 to obtain an expression which simultaneously includes the influence of yaw misalignment, wind shear, and atmospheric turbulence. Referring again to figure 1d, we can write an implicit expression for the *perturbation-dependent* local inflow angle ϕ:

$$\tan\phi = \frac{V_{r\perp}}{\Omega r + V_{r\top}} = (1+\delta)\tan\phi_0, \tag{7}$$

where the *no-perturbation* local inflow angle ϕ_0 is defined by

$$\phi_0 = \operatorname{atan}\left(\frac{\cos\beta(1-\bar{a}-K\sin\psi)}{\lambda_r - \sin\beta\cos\psi}\right), \tag{8}$$

with

$$\lambda_r = \frac{\Omega r}{U} = \frac{\Omega r}{U_\infty}\frac{\ln h_0 - \ln z_0}{\ln(h_0 + r\cos\psi) - \ln z_0} \tag{9}$$

and K as in equation 3.

Formulating the combined effect of the AOA perturbations as shown in equations 7 to 9 implies the occurrence of an atmospheric turbulent perturbation (δ) of a given magnitude is independent of the blade position (ψ, r) and misalignment angle (β). This is in agreement with international turbine certification standard [11].

2.5. From inflow angle to AOA fluctuations

We assume that the rotor does not have time to adjust the blade pitch θ to the wind speed perturbations induced by atmospheric turbulence and that the rotational speed Ω does not change during a turbulent perturbation. So those variables can be considered constant. Building on figure 1d and equation 7, we can write an expression for the *perturbation-dependent* angle of attack α:

$$\alpha = \phi - \theta = \operatorname{atan}((1+\delta)\tan\phi_0) - \theta. \tag{10}$$

Then $\alpha_0 = \phi_0 - \theta$, so a natural definition of the AOA fluctuation is

$$\alpha_\delta = \alpha - \alpha_0 = \operatorname{atan}((1+\delta)\tan\phi_0) - \phi_0. \tag{11}$$

2.6. Probability distribution function for AOA fluctuations

Since atmospheric boundary layer turbulence can be modeled as a stochastic process described by a Gaussian distribution [11], the probability density function (PDF) for the perturbation is given by

$$p(\delta) = \frac{1}{\sqrt{2\pi}I}\exp\left(-\frac{1}{2}\left(\frac{\delta}{I}\right)^2\right) \tag{12}$$

where I represents the turbulence intensity.

We derive the PDF for the AOA fluctuation from the PDF for the perturbation. For this, we first write δ as a function of α_δ starting from equation 11:

$$\delta = \frac{\tan(\phi_0+\alpha_\delta) - \tan\phi_0}{\tan\phi_0}. \tag{13}$$

Then, by applying a change of variables to the PDF for the perturbation, we get

$$\begin{aligned} q(\alpha_\delta|\psi) = \left|\frac{\mathrm{d}\delta}{\mathrm{d}\alpha_\delta}\right| p(\delta) &= \left|\frac{1+\tan^2(\phi_0+\alpha_\delta)}{\tan\phi_0}\right| p\left(\frac{\tan(\phi_0+\alpha_\delta)-\tan\phi_0}{\tan\phi_0}\right) \\ &= \frac{1}{\sqrt{2\pi}I|\tan\phi_0|}\left|1+\tan^2(\phi_0+\alpha_\delta)\right| \exp\left(-\frac{1}{2}\left(\frac{\tan(\phi_0+\alpha_\delta)-\tan\phi_0}{I|\tan\phi_0|}\right)^2\right), \end{aligned} \tag{14}$$

where in the definition of the Jacobian we made use of the fact that it is reasonable to assume $\phi_0+\alpha_\delta = \operatorname{atan}((1+\delta)\tan\phi_0) \in \left]-\frac{\pi}{2}, \frac{\pi}{2}\right[$, so that we may assume the tan function to be monotone and continuously differentiable.

The PDF of AOA fluctuation is parameterized by the turbulence intensity I and the 'no-disturbance' inflow angle ϕ_0, whose definition is given in equation 8. This angle is a function of the yaw misalignment β, the radial position r, and surface roughness z_0, and the combination of these variables may be chosen to match a specific design scenario, *e.g.* to be representative for a given turbine class.

However, ϕ_0 also depends on the azimuth angle ψ, which is used to parametrize the blade revolution. So equation 14 gives the probability density conditional on the azimuth angle. Since we know each blade position occurs cyclically and we assume the rotational speed is unchanged, the probability distribution for the azimuthal position is uniform. As such, the marginal probability of a given AOA fluctuation is obtained by performing a numerical integration of equation 14 over a revolution, i.e. for all possible values of the azimuthal angle ψ.

3. Validation of the probabilistic approach

In this section we show the comparison between the current analytical approach and an aero-structural simulation of the DTU 10 MW machine. The numerical study [13] employed the $HAWC2$ software and investigated the influence of various unsteady loading cases on the fluctuations of blade section AOA and lift coefficient C_l. Specifically, the numerical study considered tower shadow, yaw misalignment, wind shear and (a range of) turbulence intensity as fluctuation sources, in a total of 34 load scenarios. The parametric values are given in table 1 and for more detail the reader is referred to [13].

Figure 2 presents the comparison between the numerical and analytical results, in terms of the standard deviation of the AOA fluctuations. It is noted that because of the formulation presented above in section 2, the standard deviation of the *perturbation-dependent* angle of attack is the same as the standard deviation of the AOA fluctuation, *i.e.* $\sigma_\alpha = \sigma_{\alpha_\delta}$. Generally speaking, the analytical data compares reasonably well with the Aero-structural numerical results. Specifically, figure 2 shows the small slope increase of σ_α towards larger radial positions for the Wind Shear induced fluctuations in both numerical and analytical data, with similar order magnitude. Regarding the Yaw misalignment effect, results from both methods also compare favorably, with a clear trend of increasing AOA fluctuations towards inboard HAWT blade stations. Finally, figure 2 shows the effect of atmospheric turbulence is of a larger magnitude than the other perturbation sources. The trend of decreasing σ_α towards larger radial positions is clear in numerical simulation and analytical results, although the magnitude is not well captured. The differences in the magnitude of σ_α obtained with the analytical and numerical data may be attributed to the fact that no structural dynamics, unsteady aerodynamics, or tower shadow effects were included in the analytical approach. In addition, the numerical data were obtained over a certain wind speed range, whereas the analytical results consider the same (rated) wind speed.

It is noted the case study used for the comparison corresponds to representative conditions of an Offshore location in the Dutch coast, with reference turbulence corresponding to IEC [11] Class-A characteristics. As such, the magnitude of the relative fluctuatios σ_α induced by each perturbation source considered (Wind Shear $\frac{h0}{z0}$, Yaw misalignment β and atmospheric turbulence intensity I) will vary according to site specific and turbine operation characteristics.

Table 1: Numerical Simulation Parameters

Parameter	R	h_0	Ω	U_∞	z_0	β	I
Value	89 m	119 m	1 rad/s	10.6 m/s	0 m to 0.6 m	0° to 10°	0 to 0.16

4. Airfoil Optimization set-up and cost function definition

The optimization set-up and philosophy is somewhat similar to the methodology described in earlier work [7]. The airfoil design procedure is formulated as a multi-objective optimization problem, which we solve with a genetic algorithm [6]. Airfoil shapes are approximated with class and shape function parametrization [14] using 19 coefficients for the discretization. In the present article we consider airfoils representative of midspan to outboard station blades of multi MW HAWT, and as such the airfoil relative thickness is set at $t/c = 0.21$, where t denotes thickness and c represents airfoil chord. In view of manufacturability and stiffness constraints, the trailing edge region thickness of the airfoils is enforced to exceed a lower limit set at 60% of the geometry of typical wind energy airfoils with a 21 % thickness to chord ratio, approximately 3.6% t/c at a relative chordwise position $x/c = 0.7$.

Throughout the optimization two lift(L) and drag (D) polars are calculated for each airfoil candidate, corresponding to *clean* and *rough* configurations. In the *clean* configuration the transition from laminar to turbulent is left free, whereas for the *rough* case the transition is set at $x/c = 0.05$ and $x/c = 0.1$ for the upper and lower surface chord locations respectively. The aerodynamic polars are calculated using the viscous-inviscid panel method *RFOIL* [15] for a Reynolds number of $9 \cdot 10^6$—typical for large offshore HAWT. In the polar calculation the AOA ranges from 0° to 20° in steps of 0.2°.

4.1. Clean performance cost function

One of the cost functions the optimizer attempts to minimize represents the clean performance of the airfoil candidate. This is achieved by computing the expected value of the lift to drag ratio, expressed as:

$$\frac{\bar{L}}{D}(\alpha_{\mathrm{DES}}) = \int_{\alpha_{\mathrm{DES}}-1.64\sigma_{\delta_\alpha}}^{\alpha_{\mathrm{DES}}+1.64\sigma_{\delta_\alpha}} \frac{C_{\mathrm{l}}(\alpha)}{C_{\mathrm{d}}(\alpha)} p(\alpha)\,\mathrm{d}\alpha, \tag{15}$$

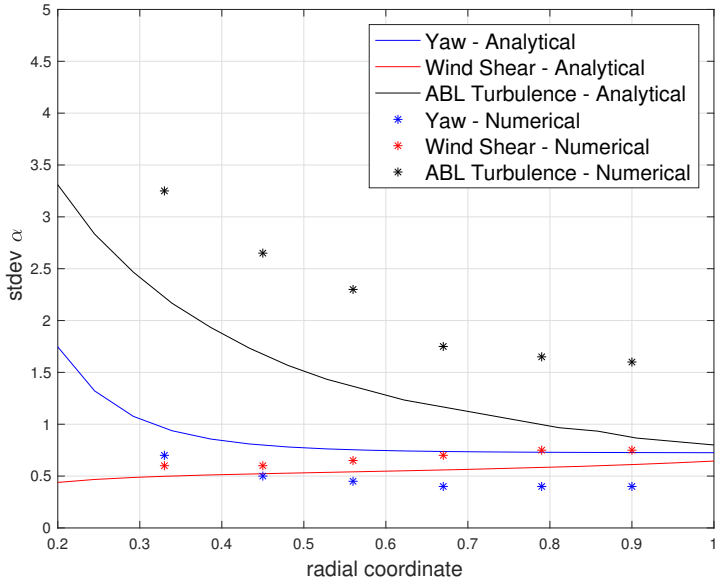

Figure 2: Comparison of AOA standard deviation obtained with analytical and numerical [13] approach

where the design angle of attack $\alpha_{\mathrm{DES}} = 7^{\circ}$ corresponds to the mid-point of the considered AOA range, thus equivalent α_0 defined in section 2. The limits of integration are chosen such that 90 % of all AOA occurrences are captured, assuming a normal probability distribution $p(\alpha)$ for AOA , that is $\alpha \approx N(\alpha_0, \sigma_\alpha)$.This approximation for the AOA probability distribution is justified on the grounds that perturbations due to atmospheric turbulence dominate over other AOA fluctuation sources (as show in figure 2) for large HAWT.

The cost function is then defined simply as:

$$CF_1 = \left. \frac{-\frac{\bar{L}}{D}(\alpha_{\mathrm{DES}})}{100} \right|_{\mathrm{clean}}, \tag{16}$$

where the minus sign is introduced as the optimizer attempts to minimize its value (and hence effectively increase aerodynamic performance).

4.2. Rough performance cost function

For the computation of the cost function representing the airfoil rough performance, an expression identical to equation 15 is employed, but naturally obtained with forced transition. Its expression is

$$CF_2 = \left. \frac{-\frac{\bar{L}}{D}(\alpha_{\mathrm{DES}})}{100} \right|_{\mathrm{rough}}. \tag{17}$$

4.3. Influence of standard deviation of AOA fluctuations on cost function computation

As described above, for each airfoil optimization, we consider a fixed value of the standard deviation of AOA fluctuations for the cost function computation, rather than explicitly using σ_α. This optimization methodology was employed such that the compromise between a point-design and a robust airfoil was highlighted. Several optimization runs were carried out using different values of σ to clearly illustrate the impact of AOA fluctuations on airfoil geometry and performance, as discussed in the results section below.

4.4. Staggered Optimization Procedure

The double objective problem was solved one time for each standard deviation of the angle of attack probability distributions. Four standard deviations were considered (0,2,4 and 6degrees) and each double-objective problem was solved in four steps:

(i) A collection of three initial guesses was generated with a gradient algorithm based on the interior point method. Results from this run were then added to the initial population of the genetic algorithm used in the next step.

(ii) The double objective problem was then tackled with the NSGA-II genetic algorithm with a population size of 160 individuals. The algorithm was allowed to run for 40 generations, and it departed from an initial population that combined 60 well known airfoil designs, the three designs generated in step 1, and 97 randomly generated designs. A pareto fraction of 45% and mutation rate of 2% were used to ensure broad coverage of the design space.

(iii) Three members of the pareto front were then drawn and fed as initial guesses to the gradient algorithm, which pushed them to extremes of the pareto front.

(iv) The double objective problem was then tackled again with the NSGA-II genetic algorithm. The algorithm was again allowed to run for 40 generations but population was increased to 200 individuals per generation and the Pareto fraction was increased to 60%. The mutation rate was maintained.

5. Optimization results and discussion

Figures 3 and 4 provide an overview of the optimization results. Figure 3 displays the Pareto fronts obtained for different standard deviation values of AOA fluctuations. Each marker along the Pareto curves represent an airfoil section.The compromise between rough and clean performance is clear along each Pareto front. This compromise may be parametrized by considering a global cost function CF_G defined with:

$$CF_G = \lambda CF_2 + (1 - \lambda)CF_1 \tag{18}$$

For an airfoil with a larger $CF1$ ($\lambda = 0$) and thus very good clean performance, rough performance is poor, corresponding to a more point-design type of airfoil [5] often associated with laminar flow airfoils [3]. Towards the right of each Pareto front ($\lambda = 1$) the difference between the *clean* and *rough* performance is much smaller, leading to a more robust type of airfoil. Robustness in this case means the airfoil performance when turbulent boundary layer (from forced transition) is forced , the performance does not degrade significantly. In practice this turbulent flow development is often caused by leading edge soiling along the blades of large HAWT.

In addition, figure 3 shows the cost function values decrease for larger values of σ_α. This results from the lower values of the expected L/D, as shown in expression 16, but also due to the fact that the optimization objectives on figure 3 show the expected value of the lift to drag ratios considering different ranges of angle of attack, thus necessarily decreasing the cost function values as larger AOA fluctuations are considered. Figure 3 also displays circle markers that correspond to the airfoil sections whose geometry and performance are shown in figure 4.

Figure 4 focuses on the region of interest of airfoil design for horizontal axis wind turbines, but recasts the optimization results to explicitly show the variation of airfoil performance with standard deviation of angle of attack. In other words, this may be interpreted as the degree of robustness, but related to good airfoil performance over a range of α.The airfoil sections and respective performance shown in figure 4 correspond to a clean/rough compromise level $\lambda = 0.5$ (illustrated by triangles in figure 3). Regarding airfoil geometry, results clearly show the trend in airfoil geometry of maximum upper thickness moving towards the leading edge as larger standard deviations of angle of attack are considered. This geometric feature in practice may lead to earlier transition from clean to rough airfoil flows [2]. As such, these results may indicate that from an airfoil design perspective, the effect of AOA fluctuations and turbulent boundary layer development *i.e.* rough conditions, is similar.

Figure 5 shows the lift and drag polars for the airfoil sections depicted in figure 4. For all presented polars a rather sharp decrease in lift is seen after C_l is maximum. This may be explained as no 'soft-stall' requirement is explicitly included in the optimizer cost functions, even though it is often used for WE airfoil optimization [7]. It can also be seen that as smaller σ are considered the minimum drag coefficient decreases, along with the 'drag bucket' range. This is to be expected as designing with smaller AOA deviations leads to a more 'point-design' type of airfoil [5].

6. Conclusion

We describe a probabilistic approach to design airfoils for a horizontal axis wind turbine, which combines the influence of wind shear, yaw-misalignment, and turbulence intensity. The probabilistic approach is incorporated into a multi-objective airfoil optimization problem and is solved with a genetic algorithm. Results illustrate the compromise between airfoil performance for a specific angle of attack and robustness of airfoil performance over an AOA range. Results suggest that from an airfoil design point of view, the effect of AOA fluctuations and turbulent boundary layer development may similar.

References

[1] Rasmussen F, Petersen J and Madsen H 1999 *Transactions of the ASME* **121** 150–155
[2] Bak C, Andersen P, Madsen H, Gaunaa M, Fuglsang P and Bove S 2008 *26th AIAA Applied Aerodynamics Conference* (Honolulu, Hawaii)
[3] Fuglsang P and Bak C 2004 *Wind Energy* **7** 145–162
[4] Leishman J 2002 *21st ASME Wind Energy Symposium* (Reno, Nevada)
[5] Liebeck R 1976 *AIAA 9th Fluid and Plasma Dynamics Conference* pp 76–406
[6] de Oliveira G 2011 *Wind turbine airfoils with boundary layer suction: a novel design approach* Master's thesis TU Delft
[7] Pereira R, Timmer W A, de Oliveira G and van Bussel G J W 2017 *Wind Energy* **20**(9) 1569–1583
[8] Schepers J G 2012 *Engineering models in wind energy aerodynamics: Development, implementation and analysis using dedicated aerodynamic measurements* Ph.D. thesis TU Delft
[9] Pitt D M and Peters D A 1981 *Vertica* **5** 21–34
[10] Manwell J, McGowan J and Rogers A 2002 *Wind energy explained: theory, design and application* (John Wiley and Sons)
[11] International Electrotechnical Comission 2005 Wind turbines - part 1: Design requirements Tech. Rep. IEC 61400-1 Edition 3.0

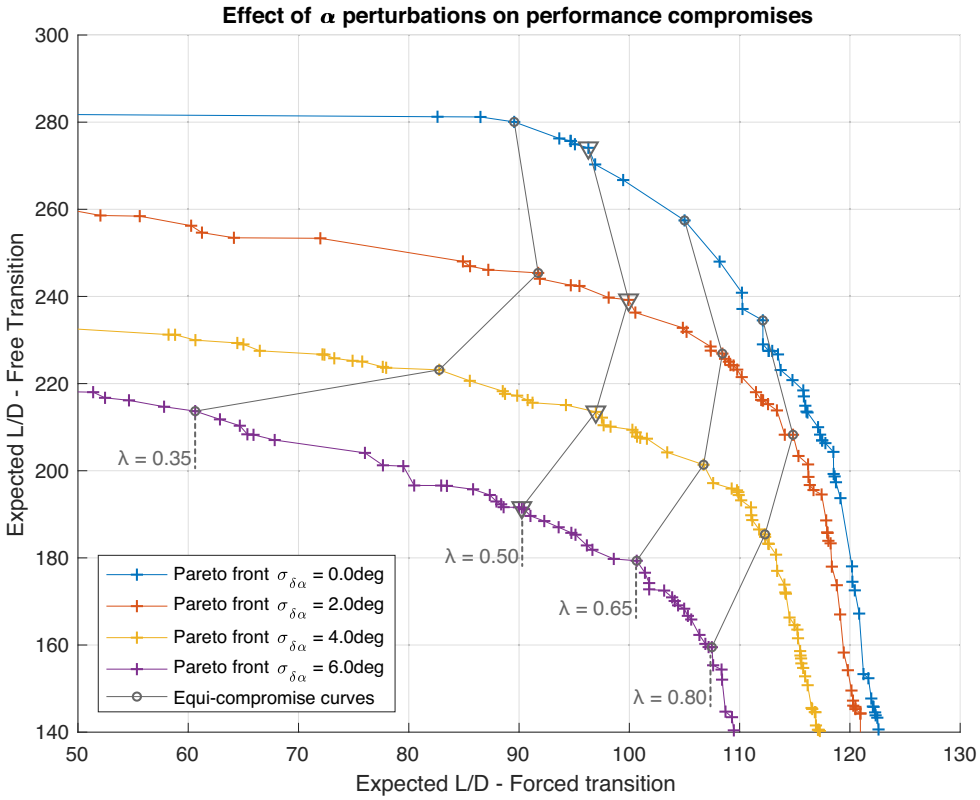

Figure 3: Optimization Results - Pareto Fronts for different σ_α

[12] Wagenaar J W and Eecen P J 2010 3D turbulence at the offshore wind farm Egmond-aan-Zee Tech. Rep. ECN-E-10-075 ECN
[13] Rezaeihaa A, Pereira R and Kotsonis M 2017 *Renewable Energy* **114**(Part B) 904–916
[14] Kulfan B M 2008 *Journal of Aircraft* **45**(1) 142–158
[15] van Rooij R 1996 Modification of the boundary layer calculation in RFOIL for improved airfoil stall prediction Tech. Rep. IW-96087R TU Delft, Institute for Wind Energy

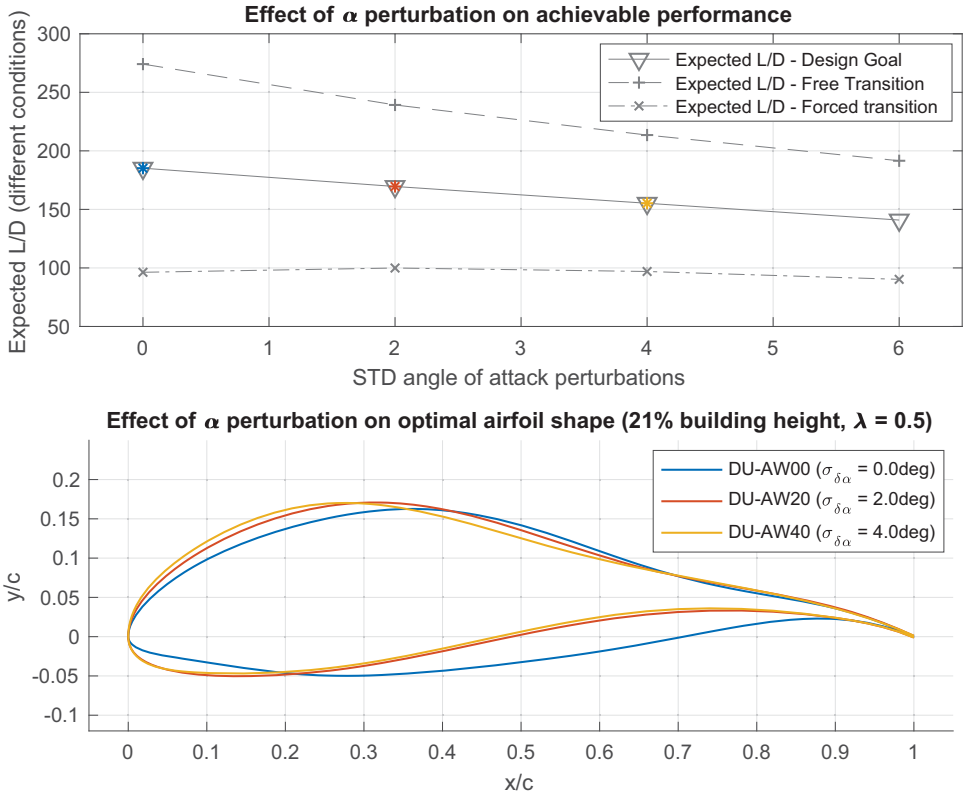

Figure 4: Optimization Results - Airfoil sections and cost function variation with AOA standadr deviation.

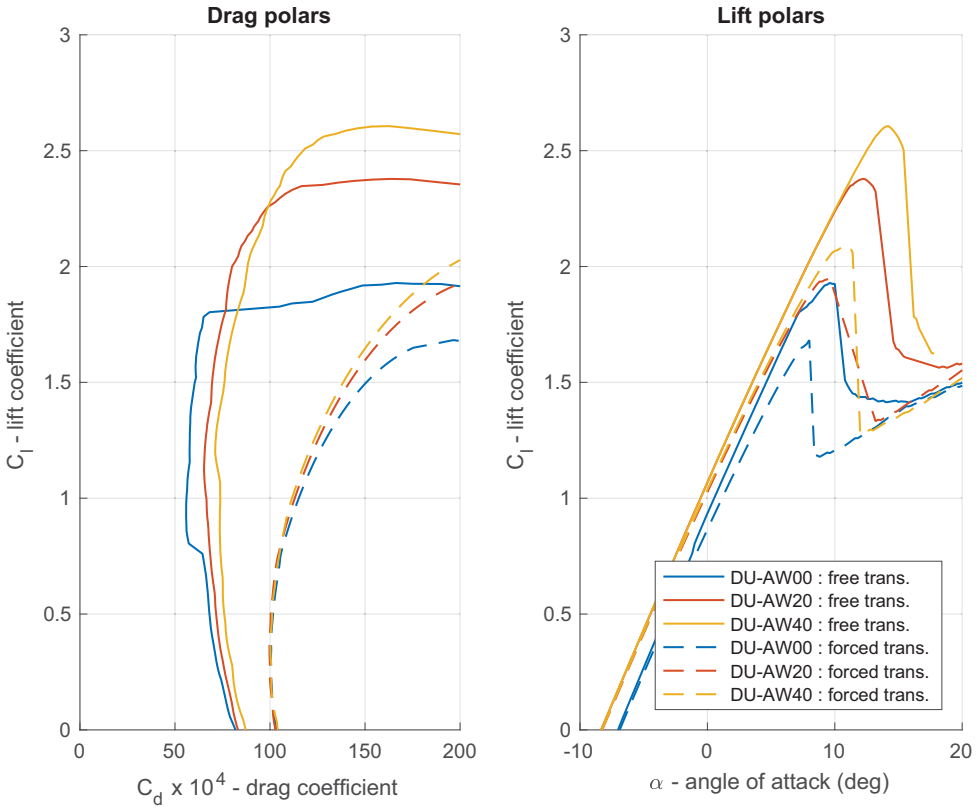

Figure 5: Lift and drag polars for the optimized airfoil sections.